

Can coupled-cluster theory treat conical intersections?

Cite as: J. Chem. Phys. **127**, 044105 (2007); <https://doi.org/10.1063/1.2755681>

Submitted: 23 April 2007 . Accepted: 12 June 2007 . Published Online: 26 July 2007

Andreas Köhn, and Attila Tajti



View Online



Export Citation

ARTICLES YOU MAY BE INTERESTED IN

[The equation of motion coupled-cluster method. A systematic biorthogonal approach to molecular excitation energies, transition probabilities, and excited state properties](#)

The Journal of Chemical Physics **98**, 7029 (1993); <https://doi.org/10.1063/1.464746>

[Excited states from modified coupled cluster methods: Are they any better than EOM CCSD?](#)

The Journal of Chemical Physics **146**, 144104 (2017); <https://doi.org/10.1063/1.4979078>

[Benchmarks for electronically excited states: CASPT2, CC2, CCSD, and CC3](#)

The Journal of Chemical Physics **128**, 134110 (2008); <https://doi.org/10.1063/1.2889385>

Lock-in Amplifiers up to 600 MHz

starting at

\$6,210



Zurich
Instruments

Watch the Video



Can coupled-cluster theory treat conical intersections?

Andreas Köhn^{a)} and Attila Tajti^{b)}

Institut für Physikalische Chemie, Universität Mainz, D-55099 Mainz, Germany

(Received 23 April 2007; accepted 12 June 2007; published online 26 July 2007)

Conical intersections between electronic states are of great importance for the understanding of radiationless ultrafast relaxation processes. In particular, accidental degeneracies of hypersurfaces, i.e., between states of the same symmetry, become increasingly relevant for larger molecular systems. Coupled-cluster theory, including both single and multireference based schemes, offers a size-extensive description of the electronic wave function, but it sacrifices the Hermitian character of the theory. In this contribution, we examine the consequences of anti-Hermitian contributions to the coupling matrix element between near-degenerate states such as linear dependent eigenvectors and complex eigenvalues. Numerical examples are given for conical intersections between two excited states calculated at the equation-of-motion coupled-cluster level which indeed show the predicted artifacts. A simple method is suggested which allows physically meaningful potential energy surfaces to be extracted from the otherwise ill-behaved results. This provides a perspective for obtaining potential energy surfaces near conical intersections at the coupled-cluster level. © 2007 American Institute of Physics. [DOI: 10.1063/1.2755681]

I. INTRODUCTION

The concept of conical intersections between electronic states is of utmost importance for the understanding of radiationless ultrafast relaxation processes.^{1–4} Conical intersections occur if two adiabatic potential energy surfaces become energetically degenerate for a given molecular conformation; the degeneracy is lifted along two orthogonal trajectories leading to a double-cone shape. Along all other degrees of freedom the degeneracy persists, giving rise to a subspace usually called intersection seam.

For a long time the appearance of conical intersections was believed to be largely symmetry driven. However, with the development of new computational techniques^{5,6} that allowed for a direct determination of the conical intersection seam it became obvious that accidental intersections of potential energy surfaces belonging to states of the same symmetry are a rather common phenomenon.⁴ In this case, the vanishing coupling between the states is not symmetry induced which leads to additional demands on the computational method. In particular, for coupled-cluster theory—which otherwise has emerged to one of the most useful tools in electronic structure theory, offering a hierarchy of size-consistent methods with increasing accuracy—problems in the vicinity of accidental degeneracies can be anticipated due to the inherent non-Hermitian character of the ansatz but are so far scarcely discussed in the literature, for an exception, see Ref. 7.

Usual coupled-cluster theory,^{8–10} relying on a single reference configuration, is not generally capable of describing intersections between the ground state and excited states. Here, multireference (MR) treatments are called for and ap-

preciable progress in the direction of applicable multireference coupled-cluster (MR-CC) schemes has been made in the recent past.^{11–14} As long as the ground state remains single-reference dominated, however, intersections between excited states are, in principle, accessible by single-reference coupled-cluster methods, via linear response (LR-CC) or, equivalently as far as energies are concerned, the equation-of-motion coupled-cluster (EOM-CC) method. Excited state intersections are of great importance for the initial relaxation dynamics after photon absorption in many systems.

The problems due to the non-Hermitian nature of the coupled-cluster approach are the same for both LR-CC/EOM-CC and multireference schemes. In the present article we will mainly focus on LR-CC/EOM-CC, although the analysis given in Sec. II is applicable to the multireference case as well, as pointed out in Sec. III. We will thereby extend the discussion of Ref. 7 and give, to our best knowledge for the first time in the literature, numerical examples for the artifacts occurring for coupled cluster in the vicinity of conical intersections (Sec. IV). A simple correction method that allows to calculate physically meaningful potential energy surfaces at conical intersections with inherently non-Hermitian methods is introduced and discussed in Sec. V.

II. TWO-STATE MODEL

A. Hermitian theory

We consider a molecule with F degrees of freedom and the corresponding electronic Hamiltonian H in the clamped nuclei approximation. The Hamiltonian depends parametrically on the molecular degrees of freedom and so do the exact eigenstates $|\Psi_i\rangle$ and eigenvalues E_i . Without loss of generality, the interaction of two close-lying states can be analyzed in a 2×2 subspace spanned by the two states of interest $|\Psi_1\rangle$ and $|\Psi_2\rangle$. At the intersection both eigenvalues

^{a)}Electronic mail: andreas.koehn@uni-mainz.de

^{b)}Present address: Institute of Chemistry, Eötvös Loránd University, P.O. Box 32, H-1518 Budapest, Hungary. Electronic mail: tat@chem.elte.hu

approach the same value. As both states are eigenvalues of the same Hamiltonian, a second condition arises which is more easily seen in the “crude diabatic basis.”^{4,15} The crude diabatic basis is obtained by an arbitrary unitary rotation U among the two eigenstates of interest, $|\tilde{\Psi}_i\rangle = U_{1i}|\Psi_1\rangle + U_{2i}|\Psi_2\rangle$. For convenience, we assume a shifted Hamiltonian, $H = H_{\text{unshifted}} - \bar{E}\mathbf{1}$, where \bar{E} is the arithmetic mean of the two excitation energies. The resulting 2×2 matrix representation can be parametrized as

$$\tilde{H} = \begin{pmatrix} \langle \tilde{\Psi}_1 | H | \tilde{\Psi}_1 \rangle & \langle \tilde{\Psi}_1 | H | \tilde{\Psi}_2 \rangle \\ \langle \tilde{\Psi}_2 | H | \tilde{\Psi}_1 \rangle & \langle \tilde{\Psi}_2 | H | \tilde{\Psi}_2 \rangle \end{pmatrix} = \begin{pmatrix} -\Delta & X \\ X & \Delta \end{pmatrix}, \quad (1)$$

assuming real matrix elements (i.e., absence of magnetic fields or spin-orbit interactions) for simplicity.

The eigenvalues of this matrix are obviously $\Lambda_{\pm} = \pm \sqrt{\Delta^2 + X^2}$. This makes clear that the degeneracy of the two states actually requires two conditions: $\Delta=0$ and $X=0$, the well-known crossing conditions of von Neumann and Wigner¹⁶ and Teller.¹⁷ As the entries in Eq. (1) depend on the F internal degrees of freedom in the molecule, it follows that the two states may be degenerate in an $(F-2)$ -dimensional subspace (crossing space, denoted \mathcal{C} hereafter, or conical intersection seam).

With approximate wave functions, the same topology is obtained, as long as the Hermiticity of the problem is not sacrificed. Non-Hermitian couplings between near-degenerate states, however, will alter the topology unless they vanish at the intersection, either due to group theoretical reasons or if the correct behavior is guaranteed, e.g., by connection to a Hermitian eigenvalue problem by a similarity transformation.

B. Non-Hermitian theory: Unphysical crossing conditions

We will start by reviewing the analysis of the general unsymmetric 2×2 subspace problem as presented in Ref. 7,

$$\begin{pmatrix} -\Delta & X+Y \\ X-Y & \Delta \end{pmatrix}. \quad (2)$$

The eigenvalues of this matrix are

$$\Lambda_{\pm} = \pm \sqrt{\Delta^2 + X^2 - Y^2}. \quad (3)$$

leading to an unphysical topology of the crossing space. The F -dimensional configuration space is partitioned into two subspaces \mathcal{F}_R and \mathcal{F}_I ; one is defined by the condition $\Delta^2 + X^2 - Y^2 > 0$ (nondegenerate real eigenvalues), and the other is defined by $\Delta^2 + X^2 - Y^2 \leq 0$ (degenerate eigenvalues or imaginary pairs). The two subspaces are separated by an $(F-1)$ -dimensional subspace for which the condition $\Delta^2 + X^2 - Y^2 = 0$ is fulfilled, which we will call enveloping space \mathcal{E} in the following. The actual crossing space \mathcal{C} , defined by $\Delta^2 + X^2 = 0$, is a subspace of \mathcal{F}_I . A conical intersection with the physically correct shape will only be observed, if $\Delta^2 + X^2 = 0$ and $Y^2 = 0$ are fulfilled separately, i.e., in an $(F-3)$ -dimensional subspace of the actual crossing space.

C. Non-Hermitian theory: Extended analysis

Most non-Hermitian theories emerge from considering the eigenvalue problem of a similarity transformed Hamiltonian $\bar{H} = W^{-1}HW$, where W is a nonsingular and nonunitary operator, usually called wave operator. If the eigenvalue problem of \bar{H} is solved in the entire basis in which W can be represented (we will refer to this case as “complete expansion”), the eigenvalue spectrum remains unchanged and consequently no problems will occur at or near intersections. However, the actual purpose of the similarity transformation is to fold physically important parts of the complete expansion into a subspace in which a reduced eigenvalue problem is solved. This means that in addition to the similarity transformation a subspace projector P is applied,

$$\bar{H}' = PW^{-1}HWP.$$

At this, the similarity transformation character is lost. Notably, both the projected and unprojected \bar{H} are unsymmetric, as $W^{-1} \neq W^\dagger$, so this property alone is not sufficient for the occurrence of the artifacts discussed above. In the following, we want to further examine the origin of the antisymmetric contributions to the coupling between two states in non-Hermitian theories.

As \bar{H} is unsymmetric, we obtain for each eigenvalue E_i different left and right eigenvectors, $|\bar{\Phi}_i\rangle$ and $|\Phi_i\rangle$. The right eigenvectors form a nonorthogonal basis with the metric

$$\langle \Phi_i | \Phi_j \rangle =: S_{ij}, \quad (4)$$

where as convention the diagonal can be chosen to be $S_{ii} = 1$. The left eigenvectors are related to the right ones by

$$|\bar{\Phi}_i\rangle = \sum_j |\Phi_j\rangle [S^{-1}]_{ji}, \quad (5)$$

and left and right states fulfill the biorthogonality relation,

$$\langle \bar{\Phi}_i | \Phi_j \rangle = \delta_{ij}. \quad (6)$$

We note that in the case of a complete expansion there exist solutions $|\Psi_i\rangle$ of the Hermitian eigenvalue problem on the same expansion space which are related to the non-Hermitian solutions by

$$|\Psi_i\rangle = N_i W |\Phi_i\rangle = \frac{1}{N_i} (W^{-1})^\dagger |\bar{\Phi}_i\rangle, \quad (7)$$

where $N_i^{-1} = \langle \Phi_i | W^\dagger W |\Phi_i\rangle \neq 1$, as usually a different normalization is used. As the $|\Psi_i\rangle$ form an orthonormal basis, it follows that

$$\langle \Phi_i | W^\dagger W |\Phi_j\rangle = N_i \delta_{ij}, \quad \langle \bar{\Phi}_i | W^{-1} (W^{-1})^\dagger |\bar{\Phi}_j\rangle = \frac{1}{N_i} \delta_{ij}. \quad (8)$$

Note, however, that the bare right eigenvectors are still non-orthogonal, i.e., $S_{ij} \neq \delta_{ij}$ in the complete expansion case. This has important consequences for the construction of correction schemes, see Sec. V.

Next, we turn to the two-dimensional subspace problem which is diagonal in the eigenvector basis,

$$\mathbf{A} = \begin{pmatrix} \langle \bar{\Phi}_1 | \bar{H} | \Phi_1 \rangle & \langle \bar{\Phi}_1 | \bar{H} | \Phi_2 \rangle \\ \langle \bar{\Phi}_2 | \bar{H} | \Phi_1 \rangle & \langle \bar{\Phi}_2 | \bar{H} | \Phi_2 \rangle \end{pmatrix} = \begin{pmatrix} \Lambda_- & 0 \\ 0 & \Lambda_+ \end{pmatrix} \\ = \begin{pmatrix} -\Lambda & 0 \\ 0 & \Lambda \end{pmatrix}. \quad (9)$$

Note that we again consider a shifted Hamiltonian such that \mathbf{A} is traceless and has either purely real or purely imaginary eigenvalues. In addition we assume that $\text{Re } \Lambda > 0$ or, respectively, $\text{Im } \Lambda > 0$. The right-hand vectors $|\Phi_1\rangle$ and $|\Phi_2\rangle$ span a nonorthogonal basis with the metric

$$\mathbf{S} = \begin{pmatrix} 1 & S \\ S & 1 \end{pmatrix} = \begin{pmatrix} 1 & \cos \varphi \\ \cos \varphi & 1 \end{pmatrix}, \quad (10)$$

where φ can be interpreted as the angle enclosed by the two vectors. So for an orthonormal case we have $\varphi = \pi/2$ and $\cos \varphi = 0$. Note, that as we constrain our analysis to real Hamiltonians, the phases of the eigenvectors can always be chosen to give a real overlap S . Next, we introduce a parametrization of the unitary matrix \mathbf{U} to transform the eigenstates in the subspace to the crude diabatic basis,

$$\mathbf{U} = \begin{pmatrix} \cos(\vartheta/2) & -\sin(\vartheta/2) \\ \sin(\vartheta/2) & \cos(\vartheta/2) \end{pmatrix}. \quad (11)$$

The appropriate transformation of \mathbf{A} into a crude diabatic basis is $\bar{\mathbf{U}} = \mathbf{S}^{1/2} \mathbf{U} \mathbf{S}^{-1/2}$, as $\mathbf{S}^{-1/2}$ orthogonalizes the right-hand basis *within* the two-dimensional subspace. The left-hand vectors are transformed by $\mathbf{S}^{1/2}$ which preserves the biorthogonality. Note, however, that the left-hand vectors are still nonorthogonal after this transformation.

The result of the transformation $\tilde{\mathbf{A}} = \bar{\mathbf{U}} \mathbf{A} \bar{\mathbf{U}}^{-1}$ has no straightforward interpretation. For our analysis it is more illuminative to consider the matrix

$$\tilde{\mathbf{A}}_o = \mathbf{S}^{-1/2} \tilde{\mathbf{A}} \mathbf{S}^{1/2} = \mathbf{U} \mathbf{S}^{-1/2} \mathbf{A} \mathbf{S}^{1/2} \mathbf{U}^\dagger \\ = \frac{\Lambda}{|\sin \varphi|} \begin{pmatrix} -\cos \vartheta & \sin \vartheta + \cos \varphi \\ \sin \vartheta - \cos \varphi & \cos \vartheta \end{pmatrix}, \quad (12)$$

i.e., we use the orthogonalized right-hand basis and the appropriate biorthogonal left-hand basis. Comparison with Eq. (2), assuming real values for Λ , suggests to identify

$$\Delta = \Lambda \frac{\cos \vartheta}{|\sin \varphi|} \text{ and } X = \Lambda \frac{\sin \vartheta}{|\sin \varphi|}. \quad (13)$$

As $S = \cos \varphi$ and

$$\Delta^2 + X^2 = \frac{\Lambda^2}{\sin^2 \varphi}, \quad (14)$$

we can write the antisymmetric contribution as

$$Y = \Lambda \frac{\cos \varphi}{|\sin \varphi|} = S \sqrt{\Delta^2 + X^2}, \quad (15)$$

and the expression for the eigenvalues becomes

$$\Lambda_\pm = \pm \Lambda = \pm \sqrt{(\Delta^2 + X^2)(1 - S^2)}. \quad (16)$$

Equation (15) relates the antisymmetric coupling directly to the nonvanishing overlap of the eigenvectors. This has the

important consequence that the antisymmetric coupling vanishes for $\sqrt{\Delta^2 + X^2} \rightarrow 0$ as long as $|S| < 1$ is fulfilled, which ensures the correct behavior at the intersection. As for the complete expansion the basis $\{|\Psi_i\rangle\}$ is complete and W is nonsingular, it follows that $\{|\Phi_i\rangle\}$ is complete as well and thus $S < 1$. We note that, if $|\Phi_1\rangle$ and $|\Phi_2\rangle$ are degenerate, any linear combination of these is a valid eigenvector and we could choose them such that $S=0$. Yet, in any neighborhood where the states are nondegenerate, S may be nonzero such that the choice $S=0$ at the degeneracy could lead to a noncontinuous behavior of S as a function of the molecular degrees of freedom.

If $|S| \rightarrow 1$, as it may be the case for truncated expansions (see Sec. IV), Λ approaches zero as well. In this case, however, the metric becomes singular; in other words, the eigenvectors of \mathbf{A} do not span the complete space. From the above it is clear that $S=1$ is equivalent to $\Delta^2 + X^2 = Y^2$ which characterizes an $(F-1)$ -dimensional subspace of the nuclear configuration space which we termed above as \mathcal{E} (enveloping space).

Going beyond this point, we have $Y^2 > \Delta^2 + X^2$ and we enter the imaginary regime. The interpretation that this means $|S| > 1$ is a bit deceptive, as we deal with normalized vectors and $-1 \leq S \leq 1$ holds strictly. In order to continue the discussion, we consider the more simple case of the matrix

$$\mathbf{A}_o^{(r)} = \mathbf{S}^{1/2} \mathbf{A} \mathbf{S}^{-1/2} = \frac{\Lambda}{|\sin \varphi|} \begin{pmatrix} -1 & \cos \varphi \\ -\cos \varphi & 1 \end{pmatrix} \\ = \begin{pmatrix} -\tilde{\Lambda} & +S\tilde{\Lambda} \\ -S\tilde{\Lambda} & +\tilde{\Lambda} \end{pmatrix} = \begin{pmatrix} -\tilde{\Lambda} & +Y \\ -Y & +\tilde{\Lambda} \end{pmatrix}, \quad (17)$$

where for the second identity the definition

$$\tilde{\Lambda} = \frac{\Lambda}{|\sin \varphi|} = \sqrt{\Delta^2 + X^2} \quad (18)$$

was introduced. The eigenvalues of the matrix are obviously $\Lambda_\pm = \pm \tilde{\Lambda} \sqrt{1 - S^2}$ and the corresponding eigenvectors read

$$\mathbf{v}_\pm = \frac{1}{\sqrt{2}} \begin{pmatrix} \cos(\varphi/2) \mp \sin(\varphi/2) \\ \cos(\varphi/2) \pm \sin(\varphi/2) \end{pmatrix}. \quad (19)$$

$\tilde{\Lambda}$ may be interpreted as the energy splitting for vanishing antisymmetric coupling. The magnitude of the antisymmetry is reflected by the overlap matrix element. In particular, we have

$$\left| \frac{Y}{\tilde{\Lambda}} \right| = |S|. \quad (20)$$

Thus, the relation $|Y| < |\tilde{\Lambda}|$ must hold strictly to avoid singularities and imaginary eigenvalues.

In the purely imaginary regime we can again start with Eq. (9) and $\Lambda = i|\Lambda|$. With a proper choice of the phases for the eigenvectors, the matrix \mathbf{S} remains real, as stated above, and we arrive at an expression for $\mathbf{S}^{1/2} \mathbf{A} \mathbf{S}^{-1/2}$ similar to Eq. (17), which is then a matrix with purely imaginary entries. We can turn this matrix into a real matrix with the same eigenvalues by dividing each element by i and interchanging the rows,

$$\begin{aligned} \mathbf{A}_o^{(i)} &= \frac{|\Lambda|}{|\sin \varphi|} \begin{pmatrix} -\cos \varphi & 1 \\ -1 & +\cos \varphi \end{pmatrix} \\ &= \begin{pmatrix} -S|\tilde{\Lambda}| & |\tilde{\Lambda}| \\ -|\tilde{\Lambda}| & +S|\tilde{\Lambda}| \end{pmatrix} = \begin{pmatrix} -\tilde{\Lambda} & +Y' \\ -Y' & +\tilde{\Lambda}' \end{pmatrix}. \end{aligned} \quad (21)$$

The eigenvalues are $\Lambda_{\pm} = \pm |\tilde{\Lambda}| \sqrt{S^2 - 1} = \pm i |\tilde{\Lambda}| \sqrt{1 - S^2}$, and the corresponding eigenvectors are

$$\mathbf{v}_{\pm} = \frac{1}{\sqrt{2}} \begin{pmatrix} e^{\mp i(\varphi/2)} \\ e^{\pm i(\varphi/2)} \end{pmatrix}. \quad (22)$$

The ratio of the antisymmetric coupling and the energy splitting of the hypothetical symmetric matrix is larger than 1,

$$\left| \frac{Y'}{\tilde{\Lambda}} \right| = \frac{1}{|S|}, \quad (23)$$

which should be compared with Eq. (20) which is valid in the real regime. In Secs. IV and V, we will use Eqs. (17) and (21) to analyze the results of numerical calculations and to derive a simple correction.

As a side note, for a complete expansion, we can, in addition, use the relation of $|\Phi_i\rangle$ and $\langle\Phi_i|$ to the solutions of the Hermitian problem, Eq. (7), and transform to a crude diabatic basis using the orthogonal (but not normalized) subspace metric,

$$\mathbf{S}' = \begin{pmatrix} N_1^2 & 0 \\ 0 & N_2^2 \end{pmatrix}, \quad \bar{\mathbf{U}}' = [\mathbf{S}']^{1/2} \mathbf{U} [\mathbf{S}']^{-1/2}. \quad (24)$$

The transformed subspace matrix then reads

$$\tilde{\mathbf{A}} = \bar{\mathbf{U}}' \mathbf{A} [\bar{\mathbf{U}}']^{-1} = \begin{pmatrix} -\Delta & (N_1/N_2)X \\ (N_2/N_1)X & \Delta \end{pmatrix}. \quad (25)$$

The asymmetry is now purely due to the different normalization factors of the states which cancel only on the diagonal. This effect is harmless, however, as the normalization constants will always be well behaved (if they become large this is only due to an inappropriate choice of the reference state which is a different problem). It rather reflects the fact that transition properties are not uniquely defined in coupled-cluster theory, as usually the normalization factors cannot be calculated in a way which is both size extensive and has nonfactorial computational scaling. These problems are discussed in a recent work on the diagonal Born-Oppenheimer correction.¹⁸ The product of the two off-diagonal elements is well defined, however, as this cancels the normalization factors.

III. A SELECTION OF COUPLED-CLUSTER METHODS

In the previous section, we considered the general wave operator W . For usual single-reference coupled-cluster theory⁸⁻¹⁰ $W = e^T$, where

$$T = T_1 + T_2 + \dots + T_n \quad (26)$$

is the cluster operator consisting of up to n -fold excitation operators with respect to the reference determinant $|0\rangle$. For

$n=2$, the method is denoted as CCSD, for $n=3$ as CCSDT, etc. The ground state energy is obtained as

$$E = \langle 0 | H e^T | 0 \rangle, \quad (27)$$

and the cluster operator is subject to the condition

$$0 = \langle \mu | e^{-T} H e^T | 0 \rangle, \quad (28)$$

where $\langle \mu |$ is an appropriately chosen projection manifold constituted by excited determinants.

For the calculation of excited states, the EOM picture is most convenient in the current context.¹⁹ One simply considers the eigenvalue problem of the similarity transformed Hamiltonian $\bar{H} = e^{-T} H e^T$ in the subspace of n -fold excitations where n is the same as chosen for the maximum excitation level of T . With these definitions, the general analysis from the previous section can be directly applied to EOM-CC, as will be done in the numerical study below. We note that the linear-response picture²⁰⁻²² provides a connection of the thus obtained excited state energies with the poles of the time-dependent coupled-cluster response function, thereby underlining the consistency of the approach.

While EOM-CC provides a multireference description of excited states, it relies on the single-reference character of the ground state wave function. If this becomes a problem, MR-CC schemes are called for. Unlike the above described single-reference CC, for which most basic theoretical problems are settled and efficient computer implementations exist, MR-CC is still in the development phase and many different approaches have been put forward.^{11-13,23,24} Substantial problems arise from the intruder state problem and therefore in recent time focus was set to state-selective methods. In way of caution it should be noted that most state-selective methods will not work properly for conical intersections, as they focus on *one* state and use an effective Hamiltonian with bias toward this state. So, strictly speaking, different Hamiltonians are solved for the two states under consideration which sacrifices the crossing conditions. Apparent intersections and avoided crossings with “ghost states” will be the consequence.

As a review of all wave function *Ansätze* available from the literature goes beyond the scope of the present work, we only give a short remark on the state-universal *Ansatz* of Jeziorski and Monkhorst.²³ The wave operator reads

$$W = \sum_{\nu} e^{T(\nu)} |\nu\rangle \langle \nu|, \quad (29)$$

where ν runs over the indices of the reference determinants under consideration. $T(\nu)$ is a cluster operator which contains excitation operators with respect to the given reference determinant. In contrast to the case of EOM-CC, the projector is directly part of the wave operator which as such is singular for that reason. The energies are obtained from the effective Hamiltonian

$$H_{\mu\nu}^{\text{eff}} = \langle \mu | H e^{T(\nu)} | \nu \rangle = \langle \mu | e^{-T(\nu)} H e^{T(\nu)} | \nu \rangle, \quad (30)$$

where the last equality holds for complete model spaces, only. Although this recovers the similarity transformation character, it is clear that there is no guarantee for a proper

behavior of H^{eff} at intersections as (a) it is projected to a subspace and (b) $T(\nu)$ is different in each column. We conclude that non-Hermiticity effects at near degeneracies are a serious issue for all coupled-cluster methods.

IV. NUMERICAL EXAMPLE: ARTIFACTS AT THE $2^1A_1/3^1A_1$ SURFACE CROSSING OF CH_2O

In the numerical part of the present work, we concentrate on EOM-CC. The test system is the $2^1A_1/3^1A_1$ surface crossing in formaldehyde, which was also considered by Dallos *et al.* at the MR-CISD level.²⁵ Here, we are not interested in locating the minimum of the intersection seam, the model system is only set up to pass through (up to some numerical precision) the intersection point as a function of one coordinate. For EOM-CCSD with an aug-cc-pVDZ basis²⁶ one appropriate choice is $r_{\text{CH}}=111.915$ pm, $\alpha_{\text{OCH}}=118^\circ$, and a variable CO bond distance (about 134.5–136.3 pm). For carrying out the calculations, some small modification of the standard solver for nonsymmetric eigenvalue problems have to be considered in order to converge complex roots. The algorithm is described in the Appendix. It works just as good as the usual Davidson-type algorithm^{27,28} for purely real roots, and converges stably, even in cases where the eigenvectors become nearly linear dependent. It was implemented in a local version of the ACES2 (Ref. 29) code and the general coupled-cluster part of LUCIA.³⁰

In Fig. 1 the results are presented in graphical form. In panel (a) we plotted the total energies (including the ground state contribution) relative to the energy at the actual intersection point which lies slightly beyond $r_{\text{CO}}=134.5$ pm. At some distance from the intersection, we still are in the \mathcal{F}_R space and a pair of real eigenvalues is found. As r_{CO} moves toward the critical region, the energies of the two states approach each other in a square-root fashion and become degenerate at the border between the region belonging to \mathcal{F}_R and \mathcal{F}_I , i.e., at the enveloping space \mathcal{E} . From panel (b) it can be seen that the eigenvectors indeed become collinear here, so the metric is singular in \mathcal{E} and the basis of eigenvectors to \bar{H} (projected) is not complete.

When approaching \mathcal{E} from \mathcal{F}_I , the imaginary contribution develops towards the singularity in same way as the real eigenvalues in \mathcal{F}_R do. The maximum imaginary contribution in the current example is 0.02 eV. Along r_{CO} , \mathcal{F}_I extends 0.7 pm; noticeable artifacts of the potential surface are found in the range of 134.7–136.1 pm. Although the extent of the region affected by the non-Hermiticity is small in the current example, it cannot be ignored as the physical crossing space (\mathcal{C}) is located right in the center of \mathcal{F}_I , i.e., $\mathcal{C} \subseteq \mathcal{F}_I$ will always hold.

Inside \mathcal{F}_I the overlap changes nearly linearly from +1 to -1 for the current example, i.e., the eigenvectors change from collinear to orthogonal (at the center) and to (antiparallel) collinear again. Note, however, that we can choose the sign of the overlap arbitrarily at each point.

Finally, we plotted the reconstructed elements of the matrix \mathbf{A}_o , Eqs. (17) and (21), $\tilde{\Lambda}$ and Y , or, respectively, in the imaginary region $\tilde{\Lambda}'$ and Y' . Noticeably, the curves are smooth when crossing \mathcal{E} although a step size of 0.0001 bohr

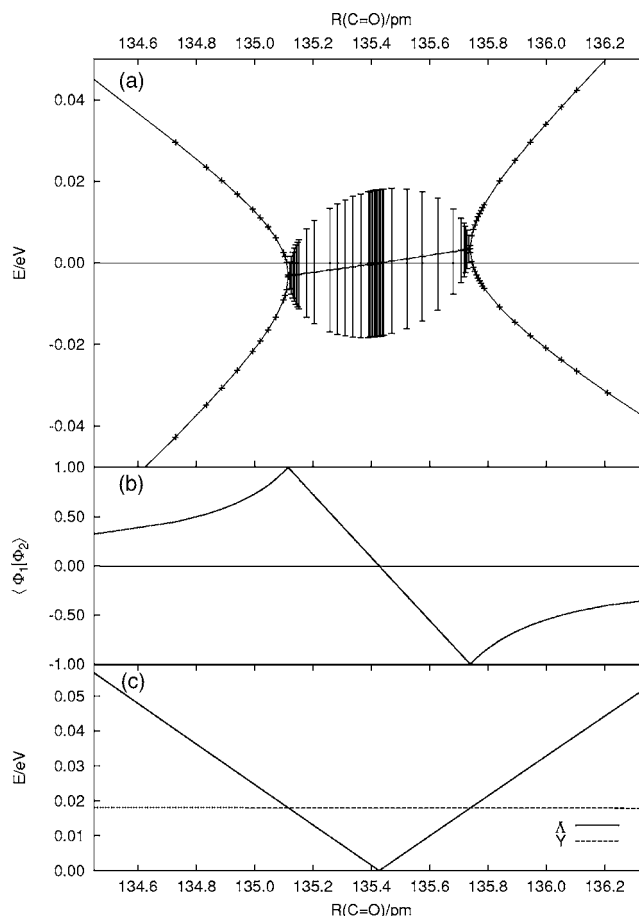


FIG. 1. Behavior of the near-degenerate solutions of EOM-CCSD for the CH_2O test system (see text) as a function of the C=O bond distance. Panel (a): Total energies of the two states relative to the energy at the intersection point. Panel (b): Overlap matrix element of the eigenvectors. Panel (c): Values of diagonal elements ($\tilde{\Lambda}$ in the regime of real splitting or $\tilde{\Lambda}'$, respectively, for imaginary splittings) and off-diagonal elements (Y or Y' , respectively) calculated according to Eqs. (17) and (21).

(~ 0.0053 pm) was chosen in these regions. The curves are remarkable, as well: $\tilde{\Lambda}$ behaves in the physically correct way; it becomes (on the present numerical scale) zero at the intersection point. Y , on the other hand, is nearly constant over the presently investigated range. The singular points occur where $\tilde{\Lambda}=Y$, as shown in Sec. II C.

V. A SIMPLE CORRECTION METHOD

One might conclude from the findings in Sec. IV that inherently non-Hermitian methods are generally not suited for the description of conical intersections. However, in the light of the otherwise excellent performance of coupled-cluster methods, it is difficult to just accept this as an irrevocable fact. In particular, the extraordinary well behaved run of $\tilde{\Lambda}$ in Fig. 1(c) suggests that physically meaningful information can be extracted from the results.

In the following we will introduce a simple correction for non-Hermitian methods which covers the special yet most common case of two close-lying states. Two observations from the previous sections will guide us:

- (a) Equation (17) gives the correct structure of the subspace matrix valid for both the approximate case and the case of a complete expansion. S does not necessarily vanish in that limit, as pointed out in Sec. II C, so symmetrization of the entire \bar{H} or of the subspace is not well founded.
- (b) The artifacts in Sec. IV occur as S assumes large values, whereas in the case of a complete expansion $|S| < 1$ is guaranteed.

From the calculations, the energies and right eigenvectors ($E_1, |\Phi_1\rangle$) and ($E_2, |\Phi_2\rangle$) are obtained. From these, the apparent half splitting $\Lambda = \frac{1}{2}(E_2 - E_1)$ and the overlap $S = \langle \Phi_1 | \Phi_2 \rangle$ are calculated. Next, we formally transform the two-dimensional subspace matrix to the form of Eq. (17), if Λ is real, or Eq. (21) if Λ is imaginary, i.e., we calculate

$$\tilde{\Lambda} = \frac{\Lambda}{\sqrt{1-S^2}} \text{ and } \left| \frac{Y}{\tilde{\Lambda}} \right| = |S|, \text{ if } \Lambda \text{ real} \quad (31)$$

or

$$\tilde{\Lambda} = \frac{S|\Lambda|}{\sqrt{1-S^2}} \text{ and } \left| \frac{Y}{\tilde{\Lambda}} \right| = \frac{1}{|S|}, \text{ if } \Lambda \text{ imaginary.} \quad (32)$$

From this, a new subspace matrix is built, which has the correct structure

$$\mathbf{A}_c = \begin{pmatrix} -\tilde{\Lambda} & \Sigma\tilde{\Lambda} \\ -\Sigma\tilde{\Lambda} & \tilde{\Lambda} \end{pmatrix} \quad (33)$$

and contains a modified overlap Σ that is a function of $|Y/\tilde{\Lambda}|$. We require that

$$\begin{aligned} \Sigma(|Y/\tilde{\Lambda}|) &\rightarrow |Y/\tilde{\Lambda}| = S, \quad \text{if } |Y/\tilde{\Lambda}| \rightarrow 0, \\ \Sigma(|Y/\tilde{\Lambda}|) &\rightarrow S_{\max} < 1, \quad \text{if } |Y/\tilde{\Lambda}| \rightarrow \infty. \end{aligned} \quad (34)$$

A possible function matching these conditions is

$$\Sigma(|Y/\tilde{\Lambda}|) = S_{\max} \tanh\left(\frac{|Y/\tilde{\Lambda}|}{S_{\max}}\right) \quad (35)$$

and the corrected eigenvalues are thus

$$\begin{aligned} \Lambda^{\text{corr}} &= \pm \tilde{\Lambda} \sqrt{1 - \Sigma^2} \\ &= \begin{cases} \pm \Lambda \frac{\sqrt{1 - \Sigma^2}}{\sqrt{1 - S^2}}, & \text{if } \Lambda \text{ real} \\ \pm (\Lambda/i) \frac{S\sqrt{1 - \Sigma^2}}{\sqrt{1 - S^2}}, & \text{if } \Lambda \text{ imaginary.} \end{cases} \end{aligned} \quad (36)$$

Already at this point, we want to stress that the specific functional form of Σ and the parameter S_{\max} is much less important for practical purposes than it might seem at first sight. In fact it will only influence the interpolation between the region well outside the conical intersection region and the conical intersection itself. Outside the conical intersection, $|Y/\tilde{\Lambda}|$ will be small (typically $\ll 10^{-1}$) and the uncorrected

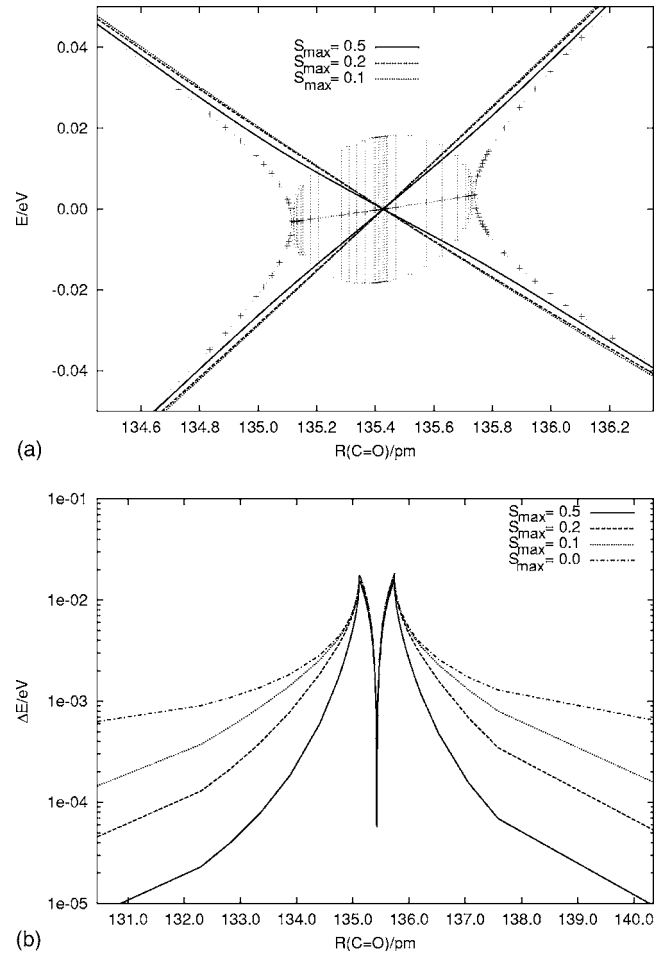


FIG. 2. Correction method applied to the $2^1A_1/3^1A_1$ intersection of CH_2O at the EOM-CCSD/aug-cc-pVDZ level. (a) Influence of different choices for S_{\max} . (b) Decay of the correction contribution ($\Lambda_c - \Lambda$); note the different scales on the x axis for (a) and (b).

method can be used. At the conical intersection, the contribution from the corrected antisymmetric coupling $Y = \Sigma\tilde{\Lambda}$ vanishes as $\tilde{\Lambda}$ goes to zero. Therefore the energy in the conical intersection seam does not depend on the chosen S_{\max} and optimizations within the conical intersection seam (the most practical scheme for investigating intersections in large molecular systems) lead to unique results.

VI. NUMERICAL TESTS OF THE CORRECTION

We first turn to the $2^1A_1/3^1A_1$ intersection of CH_2O . In Fig. 2(a), we plotted the uncorrected values (same as in Fig. 1) along with the corrected results for three different choices of S_{\max} . Only small differences result, in particular, as pointed out in the previous section, all curves coincide at the conical intersection. With $S_{\max} = 0.5$ the corrected energy follows the erratic behavior of the uncorrected curve a bit too long. The slope at the conical intersection is visibly smaller than that on the outside region, leading to a noticeable curvature. For the choices $S_{\max} = 0.2$ and $S_{\max} = 0.1$ nearly straight lines are obtained.

Figure 2(b) illustrates the decay of the corrections outside the intersection region. In addition to the above choices for S_{\max} , $S_{\max} = 0$ is included which corresponds to a com-

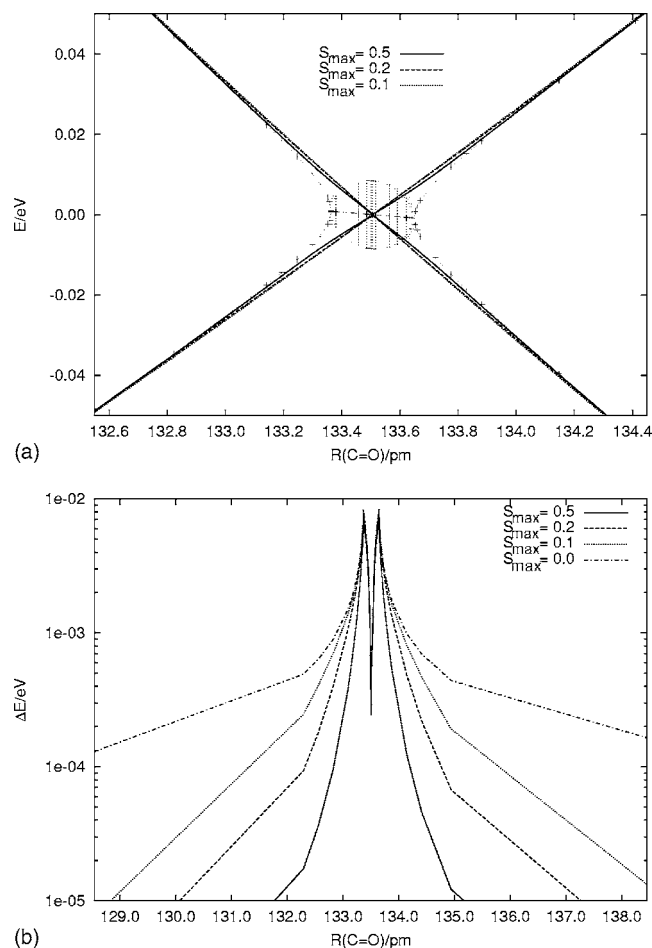


FIG. 3. Correction method applied to the $2^1A_1/3^1A_1$ intersection of CH_2O at the EOM-CCSDT/aug-cc-pVDZ level. (a) Influence of different choices for S_{max} . (b) Decay of the correction contribution ($\Delta_c - \Delta$); note the different scales on the x axis for (a) and (b). Otherwise, the same scale as in Fig. 2 was used.

plete symmetrization of the subspace or, respectively, to ignoring the antisymmetric part in Eqs. (17) and (21). This choice is theoretically not well founded, as in general $S \neq 0$ even in the limit of complete expansions (see Sec. II C). Yet, even this choice deviates from the uncorrected result by less than 10^{-3} eV at ± 3.5 pm from the conical intersection, the energy difference between the states is around 0.2 eV at this point. Much smaller deviations are obtained, if $S_{max} > 0$; in particular, for the choice $S_{max} = 0.2$ the difference to the uncorrected value at ± 3.5 pm away from the conical intersection is below 10^{-4} eV. In conclusion, for all practical purposes the suggested correction is negligible in the nondegenerate case and results from the uncorrected method can be used.

Next, we move one step up in the coupled-cluster hierarchy and redo the calculations on CH_2O for EOM-CCSDT. A bond distance $r_{CH} = 107.4$ pm and the same angle as before, $\alpha_{OCH} = 118^\circ$, were used. The region affected by the artifacts shrinks to less than 0.5 pm, as can be seen from Fig. 3(a), but the complex eigenvalues persist and hinder us from accessing the conical intersection point without resorting to our correction method. After applying the correction it becomes apparent that the chosen reaction coordinate does not

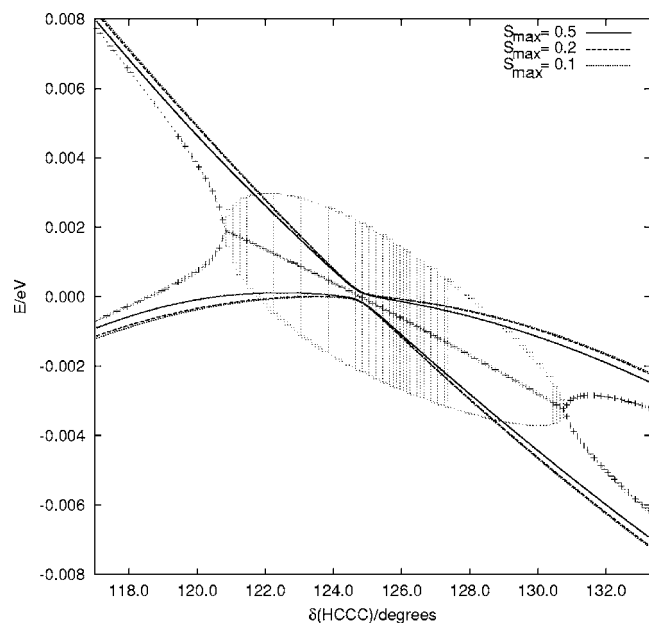


FIG. 4. Correction method applied to the (near-)intersection of the two $\pi\pi^*$ states of HCCCHO at the EOM-CCSD/cc-pVDZ level, with different choices for S_{max} .

cross the intersection for the given values; a tiny avoided crossing results. Further optimization of the other molecular parameters to find the intersection seam is computationally expensive for CCSDT and beyond the scope of the present work. As before, $S_{max} = 0.5$ leads to some additional curvature, whereas the other choices give nearly straight lines. Again, close to the intersection, here rather avoided crossing, the outcome hardly depends on the choice of S_{max} . The corrections are smaller and decay faster than those in the CCSD example, compare Figs. 2(b) and 3(b).

As a second test system we chose the $\pi - \pi^*$ states of propenal (HCCCHO). Upon excitation, the linear geometry of the triple bond is distorted; the HCC and CCC angles assume values of around 140° . The energies of the two possible $\pi - \pi^*$ excitations can now be tuned by the HCCC dihedral angle such that they interchange their energetic sequence. The corresponding EOM-CCSD surfaces calculated with the cc-pVDZ basis set are presented in Fig. 4; the precise structure parameters are available from the authors upon request. The \mathcal{F}_I region is about 10° long and, looking at the uncorrected surfaces, one cannot even decide whether we are dealing with an avoided crossing or a real intersection. Employing the correction scheme described above, a physically meaningful shape of a narrow avoided crossing can be observed with a minimum energy gap of 0.0003 eV. As above, we refrained from a further optimization of the structure parameters to find the actual conical intersection. Concerning the effect of different choices for S_{max} , the same facts can be concluded as in the case of CH_2O , in particular, close to the gap all corrected curves coincide.

Unfortunately, we are not in the position to present an example where a full expansion could be studied. From the above results it is not completely clear how the \mathcal{F}_I region develops into a physical crossing seam \mathcal{C} if the expansion becomes complete. As indicated in Sec. II C, the overlap

needs not become zero as we approach the crossing seam (although, as the vectors are degenerate, it can be chosen as zero at the crossing seam). From the CCSDT results, however, we can expect S to remain small everywhere such that the suggested correction will not significantly affect the results.

VII. SUMMARY AND CONCLUSIONS

The inherent non-Hermiticity of coupled-cluster methods, including multireference coupled cluster, leads to problems at accidental near degeneracies, i.e., near degeneracies between electronic states of the same symmetry. This has been demonstrated both theoretically and by numerical examples, the latter for the case of equation-of-motion coupled cluster (or linear-response coupled cluster, respectively).

Here, we concentrated on the special, but most common, case of two interacting states. As pointed out before in the literature,⁷ for a given pair of interacting states the F -dimensional nuclear configuration space \mathcal{F} can be divided into regions where real eigenvalues are obtained, here denoted \mathcal{F}_R , and regions with complex eigenvalues, \mathcal{F}_I . The former can be characterized by the condition that half the energy splitting arising from the Hermitian part of the interaction matrix, called $\tilde{\Lambda}$, is larger than the anti-Hermitian interaction matrix element Y . For the latter $\tilde{\Lambda} < Y$ holds. In an $(F-1)$ -dimensional subspace of \mathcal{F} , the antisymmetry equals the energy splitting, $\tilde{\Lambda} = Y$, leading to linear dependent eigenvectors and thus to a singular metric. This space was termed enveloping space \mathcal{E} as it surrounds the part of the configuration space in which complex eigenvalues occur.

A relation between the antisymmetric coupling element and the overlap matrix element of the two eigenvectors of the nonsymmetric eigenvalue problem was derived which facilitates the analysis of numerical calculations. Also, a slight modification of the usual Davidson-type algorithm employed in the solution of nonsymmetric eigenvalue problems was described (see appendix), which allows to converge complex roots. No modification of the underlying routines to calculate the matrix-vector product is needed. These developments enabled numerical studies on excited state surface crossing in formaldehyde and propinal, which indeed show the predicted artifacts.

A simple correction method is put forward which provides real and smooth hypersurfaces with the correct topology at the conical intersection. It works as an *a posteriori* correction and imposes the condition $|Y| < |\tilde{\Lambda}|$ in order to ensure that the antisymmetric coupling vanishes for zero energy splitting, as it should in the exact case. It reproduces the uncorrected values if it is sufficiently far away from the conical intersection and is thus compatible with conventional results obtained at other regions of the nuclear configuration space. The energy at the conical intersection does not depend on the choice of the functional form for the modified Y , which influences the interpolation between the intersection and the outside region only. Optimizations within the intersection seam thus lead to unique results.

The method is potentially unstable at the singular points, i.e., in the enveloping space. However, no effect from this was experienced in present test applications but the issue will be monitored in future developments. As a next step, a Lagrange formulation of the correction is to be developed which then allows to derive expressions for gradients and gradient coupling vectors. With this, the location and optimization of conical intersection seams at the coupled-cluster level will come into reach.

ACKNOWLEDGMENTS

This work was supported by the Deutsche Forschungsgemeinschaft. One of the authors (A.T.) acknowledges support by EU training and research network NANOQUANT, Contract No. MRTN-CT-2003-506842.

APPENDIX: A MODIFIED DAVIDSON ALGORITHM FOR THE TREATMENT OF IMAGINARY PAIRS

The time-consuming step in solving the eigenvalue problem of \bar{H} for the lowest few eigenvectors is the calculation of the matrix-vector product,

$$\bar{H}|b_i\rangle = |\bar{H}b_i\rangle. \quad (\text{A1})$$

This step is usually implemented for real arithmetic only. However, as the trial vector enters linearly, with a few minor modifications, all present quantum chemistry codes can be adapted to solve the EOM-CC equations for imaginary roots, provided that they are able to treat at least two eigenvectors at a time.

From a given set of trial vectors $\{|b_i\rangle\}$ a subspace matrix,

$$\mathbf{M} = (M_{ij}) = (\langle b_i | \bar{H} b_j \rangle), \quad (\text{A2})$$

is constructed and the right-hand eigenvalue problem is solved in the subspace

$$\mathbf{M}\mathbf{c}_i = \epsilon_i \mathbf{c}_i. \quad (\text{A3})$$

Here, ϵ_i is the current eigenvalue approximation and the current approximation to the solution vector in the full basis is

$$|v_i\rangle = \sum |b_j\rangle c_{ji}. \quad (\text{A4})$$

As \mathbf{M} is real valued by construction, imaginary roots appear as pairs, and without loss of generality we assume $\epsilon_i = \epsilon_{i+1}^*$. Furthermore, we can choose the phases of eigenvectors such that the two conditions

$$\mathbf{c}_i = \mathbf{c}_{i+1}^* \quad \text{and} \quad S = \mathbf{c}_{i+1}^\dagger \mathbf{c}_i, \quad \text{real} \quad (\text{A5})$$

are fulfilled which is convenient in the further steps.

In order to have real arithmetics in the matrix-vector product step, we separate real and imaginary contributions,

$$\epsilon_i = \epsilon_i^{(r)} + i\epsilon_i^{(i)} \quad \text{and} \quad \mathbf{c}_i = \mathbf{c}_i^{(r)} + i\mathbf{c}_i^{(i)}. \quad (\text{A6})$$

Note that the real and imaginary parts of $|v_i\rangle$ are spanned in the same basis of trial vectors. The real and imaginary parts of the residual can be calculated as

$$|r_i^{(r)}\rangle = \sum_j [(\bar{H}b_j) - \epsilon_i^{(r)}|b_j\rangle]c_{ji}^{(r)} + \epsilon_i^{(i)}|b_j\rangle c_{ji}^{(i)}, \quad (\text{A7})$$

$$|r_i^{(i)}\rangle = \sum_j [(\bar{H}b_j) - \epsilon_i^{(r)}|b_j\rangle]c_{ji}^{(i)} - \epsilon_i^{(i)}|b_j\rangle c_{ji}^{(r)}. \quad (\text{A8})$$

As the residuals for both vectors of the complex pair can be constructed from this, considering the real and imaginary components separately is sufficient. The new trial vectors are obtained as usual by preconditioning of the above residuals and orthogonalization to the present subspace.

¹G. A. Worth and L. S. Cederbaum, *Annu. Rev. Phys. Chem.* **55**, 127 (2004).

²M. Olivucci and A. Migani, in *Conical Intersections: Electronic Structure, Dynamics and Spectroscopy*, edited by W. Domcke, D. Yarkony, and H. Köppel (World Scientific, Singapore, 2004).

³F. Bernardi, M. Olivucci, and M. A. Robb, *Chem. Soc. Rev.* **25**, 321 (1996).

⁴D. R. Yarkony, *Rev. Mod. Phys.* **68**, 985 (1996).

⁵M. J. Bearpark, M. A. Robb, and H. B. Schlegel, *Chem. Phys. Lett.* **223**, 269 (1994).

⁶M. R. Manaa and D. R. Yarkony, *J. Chem. Phys.* **99**, 5251 (1992).

⁷C. Hättig, *Adv. Quantum Chem.* **50**, 37 (2005).

⁸R. J. Bartlett, in *Modern Electronic Structure Theory*, edited by D. R. Yarkony (World Scientific, Singapore, 1995), Vol. 2, Chap. 16, pp. 1047–1131.

⁹R. J. Bartlett, *J. Phys. Chem.* **93**, 1697 (1989).

¹⁰T. Helgaker, P. Jørgensen, and J. Olsen, *Molecular Electronic-Structure Theory* (Wiley, New York, 2000).

¹¹X. Li and J. Paldus, *J. Chem. Phys.* **119**, 5320 (2003).

¹²U. S. Mahapatra, B. Datta, and D. Mukherjee, *J. Chem. Phys.* **110**, 6171 (1999).

¹³M. Hanrath, *J. Chem. Phys.* **123**, 084102 (2005).

¹⁴F. A. Evangelista, W. D. Allen, and H. F. Schaefer III, *J. Chem. Phys.* **125**, 154113 (2006).

¹⁵H. C. Longuet-Higgins, *Adv. Spectrosc. (N.Y.)* **2**, 429 (1961).

¹⁶J. von Neumann and E. Wigner, *Phys. Z.* **30**, 467 (1929).

¹⁷E. Teller, *J. Phys. Chem.* **41**, 109 (1936).

¹⁸J. Gauss, A. Tajti, M. Kállay, J. F. Stanton, and P. G. Szalay, *J. Chem. Phys.* **125**, 144111 (2006).

¹⁹J. F. Stanton and R. J. Bartlett, *J. Chem. Phys.* **98**, 7029 (1993).

²⁰H. J. Monkhorst, *Int. J. Quantum Chem.* **S11**, 421 (1977).

²¹H. Koch and P. Jørgensen, *J. Chem. Phys.* **93**, 3333 (1990).

²²H. Koch, H. J. A. Jensen, P. Jørgensen, and T. Helgaker, *J. Chem. Phys.* **93**, 3345 (1990).

²³B. Jeziorski and H. J. Monkhorst, *Phys. Rev. A* **24**, 1668 (1981).

²⁴J. Pittner, *J. Chem. Phys.* **118**, 10876 (2003).

²⁵M. Dallos, H. Lischka, R. Shepard, D. R. Yarkony, and P. G. Szalay, *J. Chem. Phys.* **120**, 7330 (2004).

²⁶R. A. Kendall, T. H. Dunning, and R. J. Harrison, *J. Chem. Phys.* **96**, 6796 (1992).

²⁷E. R. Davidson, *J. Comput. Phys.* **17**, 87 (1975).

²⁸K. Hirao and H. Nakatsuji, *J. Comput. Phys.* **45**, 246 (1982).

²⁹J. F. Stanton, J. Gauss, J. D. Watts, P. G. Szalay and R. J. Bartlett, ACES II, an *ab initio* program system, 2006, with contributions from A. A. Auer, D. B. Bernholdt, O. Christiansen *et al.*, and the integral packages MOLECULE (J. Almlöf and P. R. Taylor), PROPS (P. R. Taylor), and ABACUS (T. Helgaker, H. J. Aa. Jensen, P. Jørgensen, and J. Olsen). For the current version, see <http://www.aces2.de>

³⁰J. Olsen and A. Köhn, LUCIA, a configuration interaction and coupled cluster program, University of Aarhus, 2004.